

# Magnetic Configuration and Heating Location Dependences of Toroidal Torques by Electron Cyclotron Heating in LHD<sup>\*)</sup>

Yasuhiro YAMAMOTO and Sadayoshi MURAKAMI

*Department of Nuclear Engineering, Kyoto University, Kyoto 615-8540, Japan*

(Received 17 November 2020 / Accepted 28 January 2021)

Toroidal torque by electron cyclotron heating (ECH) is investigated in the Large Helical Device (LHD) plasmas, assuming the supra-thermal electrons by ECH generate torques on the plasma through  $j_r \times B$  and collisions. The  $j_r \times B$  torque depends on the radial drift velocity and the fraction of trapped electrons. Therefore, the magnetic configuration and the heating location affects the toroidal torque. We investigate the magnetic configuration and heating location dependences of toroidal torques by ECH in LHD, by considering three typical magnetic configurations: the inward shifted, standard, and outward shifted configurations. As a result, magnetic ripple bottom heating generates larger torque than that of ripple top heating because of the large fraction of trapped electrons. Also, heating at the outer minor radius generates larger toroidal torque than that of heating at the inner radius, and the injection angle can also change the toroidal torque profile. Moreover, ECH generates the largest toroidal torque in the outward shifted configuration. Finally, we evaluate the toroidal flow velocities with the obtained toroidal torques. We obtained the largest flow near the axis in the standard configuration because of its small viscosity and large toroidal torque.

© 2021 The Japan Society of Plasma Science and Nuclear Fusion Research

Keywords: toroidal flow, ECH, LHD, magnetic configuration, torque, rotation

DOI: 10.1585/pfr.16.2403043

## 1. Introduction

Toroidal flow is an important issue in turbulence transport and magnetohydrodynamic stability. Recently, spontaneous toroidal flows driven by electron cyclotron heating (ECH) have been observed in many tokamaks and helical devices such as JT-60U, LHD, and HSX. Many experimental [1, 2] and theoretical [3] studies have been undertaken to clarify the underlying mechanism. However, the mechanism of the toroidal flow generation by ECH has not yet been understood well.

We previously reported that ECH could apply torques on the plasma through  $j_r \times B$  and collisions [6, 7]. Also, the  $j_r \times B$  torque overcomes the collisional torque in the non-symmetric configuration. Therefore, the  $j_r \times B$  torque would be a candidate for the torque driving the toroidal flow.

In LHD, toroidal flows have been investigated in Neutral Beam Injection (NBI) heating and ECH plasmas, where the toroidal flow velocity is measured by the charge exchange recombination spectroscopy (CXRS) [4, 5]. Also, LHD has flexibility on the magnetic configuration by shifting the magnetic axis. It is known that the confinement of energetic particles of the inward shifted configuration is better than that of the outward shifted configuration due to the trapped particle orbit improvement. Figure 1 shows the orbits of a helically trapped electron

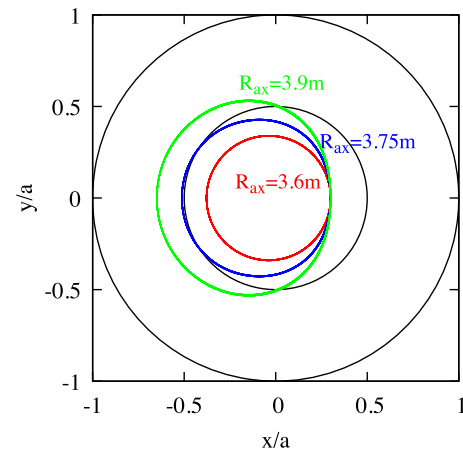


Fig. 1 The orbits of helically trapped electrons with the energy  $E = 5$  keV and the pitch angle  $\theta_p = 87^\circ$  in the inward shifted configuration (red), the standard configuration (blue) and the outward shifted configuration (green). The initial position is set at  $(r/a = 0.3, \theta = 0^\circ, \phi = 18^\circ)$ .

with the kinetic energy  $E = 5$  keV and the pitch angle  $\theta_p = \arccos(v_{\parallel}/v) = 87^\circ$  in the inward shifted configuration ( $R_{ax} = 3.6$  m), the standard configuration ( $R_{ax} = 3.75$  m), and the outward shifted configuration ( $R_{ax} = 3.9$  m). The orbit width is the smallest in the inward shifted configuration and the largest in the outward shifted configuration. Actually, the magnetic configuration near the axis of the inward shifted configuration is close to axisymmetry. There-

author's e-mail: yamamoto\_y@p-grp.nucleng.kyoto-u.ac.jp

<sup>\*)</sup> This article is based on the presentation at the 29th International Toki Conference on Plasma and Fusion Research (ITC29).

fore, we expect the  $j_r \times B$  torque would be significant in the outward shifted configuration because the radial diffusion of trapped electrons is important for the  $j_r \times B$  torque. Also, the heating location varies the fraction of trapped supra-thermal electrons accelerated by ECH. The heating location dependence on the  $j_r \times B$  torque would appear through the fraction of trapped electrons. Additionally, including the finite parallel wavenumber, the resonance condition is shifted due to the Doppler effect, and the change of the heating source profile would appear in velocity space.

In this study, we investigate the dependences of magnetic configuration and heating location on toroidal torque by ECH in LHD, by applying the GNET code, which can solve a linearized drift kinetic equation for  $\delta f$  electrons by ECH in 5-D phase space [8]. Also, we evaluate the toroidal flow velocities driven by the ECH torques, by solving the diffusion equation of toroidal flow.

## 2. Simulation Model

To investigate the electron velocity distribution and the toroidal torque due to ECH, we apply the GNET code, which can solve the drift kinetic equation in 5-D phase space using the Monte Carlo method. We split the gyrophase averaged electron distribution function  $f$  into a stationary Maxwellian part  $f_{\text{Max}}$  and an perturbed part by ECH  $\delta f$  as  $f = f_{\text{max}} + \delta f$ . The drift kinetic equation for  $\delta f$  is given by

$$\frac{\partial \delta f}{\partial t} + (\mathbf{v}_d + \mathbf{v}_{\parallel}) \cdot \frac{\partial \delta f}{\partial \mathbf{r}} + \dot{\mathbf{v}} \cdot \frac{\partial \delta f}{\partial \mathbf{v}} - C(\delta f) - L(\delta f) = S^{\text{ql}}(f_{\text{max}}), \quad (1)$$

where  $\mathbf{v}_{\parallel}$  and  $\mathbf{v}_d$  are the velocity parallel to the magnetic field and the drift velocity, respectively. Also,  $C(\delta f)$ ,  $L(\delta f)$  and  $S^{\text{ql}}(f_{\text{max}})$  are the collision operator, the orbit loss term, and the heating source term of ECH, respectively. In GNET, we can take into account the pitch angle scattering, the energy slowing down due to collisions, and the complex orbit effect in the three-dimensional magnetic configuration. We note that we can investigate the effect of  $\delta f$  electrons, which is distorted from the Maxwellian by ECH, and the GNET simulation results are separated from the neoclassical transport of the bulk ions and electrons.

The ECH source term is described by the quasi-linear diffusion theory. We consider only the linear effect  $S^{\text{ql}}(f_{\text{max}})$  for simplicity. Then the source term  $S^{\text{ql}}$  is expressed as

$$S^{\text{ql}}(f_{\text{max}}) = -\frac{\partial}{\partial v_i} D_{ij}^{\text{ql}} \frac{\partial f_{\text{max}}}{\partial v_j}, \quad (2)$$

where  $D_{ij}^{\text{ql}}$  is the quasi-linear diffusion tensor and the radial profile of the absorption power density is set as a Gaussian distribution. We consider that the right-handed electric field of the electron cyclotron (EC) wave is dominant for the X-mode. Under this limitation, we obtain [9, 10]

$$S_X^{\text{ql}} = \frac{D_{\text{ECH}}^{\text{ql}}}{v_{\perp}} \frac{\partial}{\partial v_{\perp}} \left[ v_{\perp} \left( \frac{v_{\perp}}{v_{\text{the}}} \right)^{2(n-1)} \right]$$

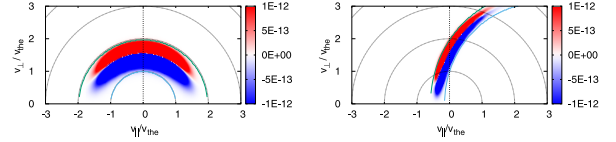


Fig. 2 Heating sources using the quasi-linear diffusion theory of X-mode ECH with  $N_{\parallel} = 0$  (left) and  $N_{\parallel} = 0.4$  (right). The velocity is normalized by the thermal velocity of 4 keV,  $v_{\text{the}}$ .

$$\times \delta \left( \omega - \frac{n\Omega_{ce}}{\gamma} - \frac{N_{\parallel}\omega v_{\parallel}}{c} \right) \frac{\partial f_{\text{max}}}{\partial v_{\perp}}, \quad (3)$$

where  $n$ ,  $\omega$ ,  $N_{\parallel}$ ,  $\Omega_{ce}$ ,  $\gamma$  and  $D_{\text{ECH}}^{\text{ql}}$  are the harmonic number of the resonance, the wave frequency, the parallel refractive index of the EC wave, the cyclotron frequency of electrons, the Lorentz factor of electrons, and the constant value, respectively. Typical cases of the quasi-linear source term with parameters ( $N_{\parallel} = 0$ ,  $n\Omega_{ce}/\omega = 1.02$ ,  $T_e = 4$  keV) and ( $N_{\parallel} = 0.4$ ,  $n\Omega_{ce}/\omega = 1.02$ ,  $T_e = 4$  keV) are shown in Fig. 2, which indicates heating from the blue region to the red region in velocity space. Here, the parameters  $N_{\parallel}$  and  $n\Omega_{ce}/\omega$  are important to determine the resonance condition  $\omega = n\Omega_{ce}/\gamma + N_{\parallel}\omega v_{\parallel}/c$ . With perpendicularly injected ECH ( $N_{\parallel} = k_{\parallel}c/\omega = 0$ ), the line of the resonance condition draws a circle whose center is ( $v_{\parallel} = 0$ ,  $v_{\perp} = 0$ ). With obliquely injected ECH ( $N_{\parallel} = 0.4$ ), the resonance circle is shifted due to the Doppler effect. Here, the strength of  $S^{\text{ql}}$  shown in the Fig. 2 cannot be compared because the parameter  $D_{\text{ECH}}^{\text{ql}}$  is not included here.

ECH applies torques on the plasma through  $j \times B$  and collisions. Since the radial movements of trapped electrons accelerated by ECH are faster than those of thermal electrons, ECH can drive the radial electron current  $j_e$ . The net current in the steady state should vanish to maintain the quasi-neutrality, so the return current,  $j_r (= -j_e)$ , must flow in the bulk plasma. Therefore, the bulk plasma feels  $j_r \times B$  torque due to the return current. On the other hand, during the slowing down of the energetic electrons, they transfer their momenta to the bulk plasma due to collisions, which is referred to as the collisional torque. We evaluate the momentum exchange between  $\delta f$  electrons and bulk plasmas as the collisional torque. In the GNET code, the toroidal component of the collisional torque density,  $T_{\phi}^{\text{col}}$ , is calculated as

$$T_{\phi}^{\text{col}}(\rho_i) = R^2 \sum_{n=1}^{n_{\text{max}}} w_n \Delta p_{\parallel, n} \mathbf{b} \cdot \nabla \phi / \Delta V(\rho_i), \quad (4)$$

where  $\rho_i$ ,  $R$ ,  $\phi$ ,  $\mathbf{b}$ ,  $\Delta V$ ,  $w_n$  and  $\Delta p_{\parallel, n}$  are the normalized minor radius of the  $i$ -th radial grid, the major radius, the toroidal angle, the unit vector in the direction of the magnetic field, the volume of the  $i$ -th radial grid, the weight of the  $n$ -th test particle, which is determined by the ECH absorption power, and the change of the parallel momentum of the  $n$ -th test particle due to collisions, respectively. The

summation is taken over the number of test particles in the  $i$ -th radial grid,  $n_{\max}$ . If we consider the heating source without initial momentum input, such as the ECH source of  $N_{\parallel} = 0$  (Fig. 2 (left)), the collisional torque of the particles passing in the co-direction should be equal to that of the particles passing in the counter-direction. The trapped particles, however, have precession motion, which can contribute to the net collisional torque. The  $j_r \times B$  and collisional torques driven by the heating source without initial momentum input should cancel in the completely symmetric configuration in the symmetry direction except for the effect of the transient orbit width [11, 12]. Therefore, the conservation of angular momentum is satisfied, and the total toroidal torque should vanish in the axisymmetric configuration. However, non-symmetric magnetic modes enhance the radial electron flux and break the cancellation of the two torques. Since the  $j_r \times B$  torque is dominant in LHD, the ECH torque is subject to the radial drift velocity of trapped electrons and the fraction of trapped electrons.

### 3. Results

Applying GNET code, we solve the linearized drift kinetic equation for the supra-thermal electrons in 5D phase space and evaluate the deviation of the distribution function from the Maxwellian,  $\delta f$ , in the inner shifted ( $R_{ax} = 3.6$  m), standard ( $R_{ax} = 3.75$  m) and outward shifted ( $R_{ax} = 3.9$  m) configurations. We assume an ECH plasma with the central electron temperature  $T_{e0} = 4$  keV, the central ion temperature  $T_{i0} = 1$  keV and the central electron density  $n_{e0} = 1 \times 10^{19} \text{ m}^{-3}$ . Also, the toroidal magnetic field is  $B_t = 1.375$  T. Figure 3 shows the isosurface plots of the velocity distribution averaged over the flux-surface  $\delta f(v_{\parallel}, v_{\perp}, r/a)$ . Left figures are  $\delta f$  by the magnetic ripple top ( $r/a = 0.2$ ,  $\theta = 180^\circ$ ,  $\phi = 0^\circ$ ) heating and right figures are  $\delta f$  the magnetic ripple bottom ( $r/a = 0.2$ ,  $\theta = 0^\circ$ ,  $\phi = 18^\circ$ ) heating in the three configurations. In the ripple top heating case, most electrons are initially passing particles and need the pitch angle scattering before radial movement. On the other hand, in the ripple bottom heating case, most electrons are initially trapped, and easily move radially. In the top heating case, we can find more electrons around the heating location ( $r/a \sim 0.2$ ) in the low perpendicular velocity region ( $v_{\perp} \sim 0$ ), where there is little acceleration in the quasi-linear source term. It indicates that the electrons actually get pitch angle scattering before the radial movement, and the resulting radial movement during the thermalization is shorter in the top heating case than that in the bottom heating case. The difference is clear in the standard configuration, as shown in Figs. 3 (c) and (d). In the bottom heating case, the trapped electrons move radially before pitch angle scattering and energy slowing down, and they get thermalized after the radial movement. Especially, in the outward shifted configuration, the supra-thermal electrons tend to go to the last closed flux surface without enough energy slowing down. In the inward

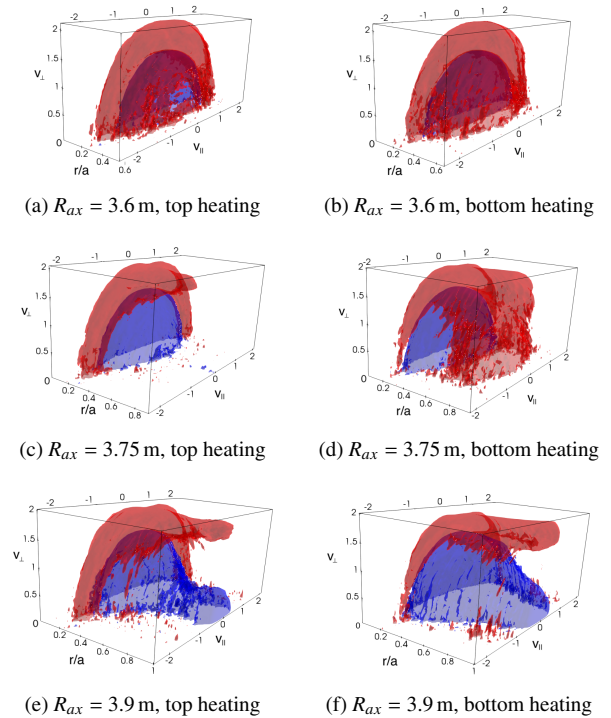


Fig. 3 Isosurface plots of the deviation of the velocity distribution  $\delta f$  from the Maxwellian. Left figures are those for the magnetic ripple top heating cases and right figures are those for the magnetic ripple bottom heating cases (a) and (b) in the inward shifted configuration, (c) and (d) in the standard configuration and (e) and (f) in the outward shifted configuration. Also, the velocity  $v_{\parallel}$  and  $v_{\perp}$  are normalized by thermal velocity.

shifted configuration, the tendency is the same, but the difference between ripple top heating and ripple bottom heating is small. Also, the result of the standard configuration is in between those of the inward and outward configurations.

We investigate the heating location dependence of the total torque, which includes the  $j_r \times B$  and collisional torque. The total toroidal torque profiles with different heating location ( $r/a = 0.1, 0.3, 0.5, 0.7$ , and ripple top ( $\theta = 180^\circ$ ,  $\phi = 0^\circ$ ) or ripple bottom ( $\theta = 0^\circ$ ,  $\phi = 18^\circ$ )) and the integrated toroidal torque for each heating location are shown in Fig. 4. Here, the EC wave is assumed to be injected perpendicularly. Ripple bottom heating generates larger net toroidal torque than top heating because of the fraction of trapped electrons. Also, heating at the outer minor radius generates larger toroidal torque than that by heating at the inner minor radius due to the strong magnetic ripple. The integrated toroidal torques by ripple top heating vary moderately with different minor radii of the heating location than those by ripple bottom heating. The difference between the top and bottom heating is comparatively small in the inward shifted configuration. The outward shifted configuration generates larger toroidal torque in the case of heating at the inner minor radii because

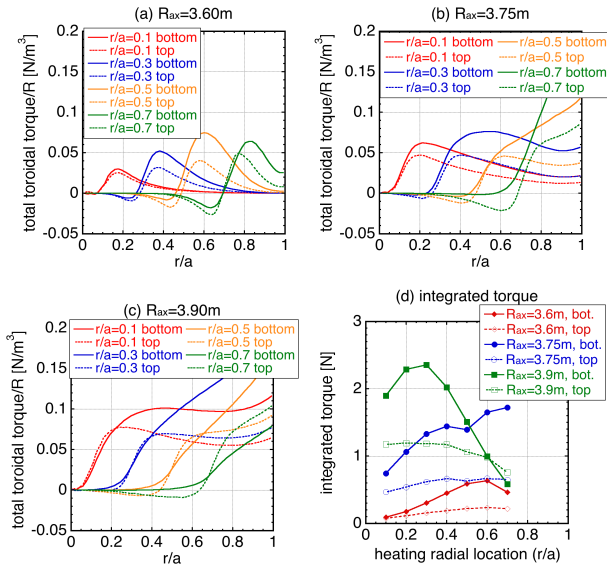


Fig. 4 The toroidal torque profiles with different heating location in (a) the inward shifted configuration, (b) the standard configuration and (c) the outward shifted configuration. (d) Dependences of the heating location and the configuration on the integrated ECH torque.

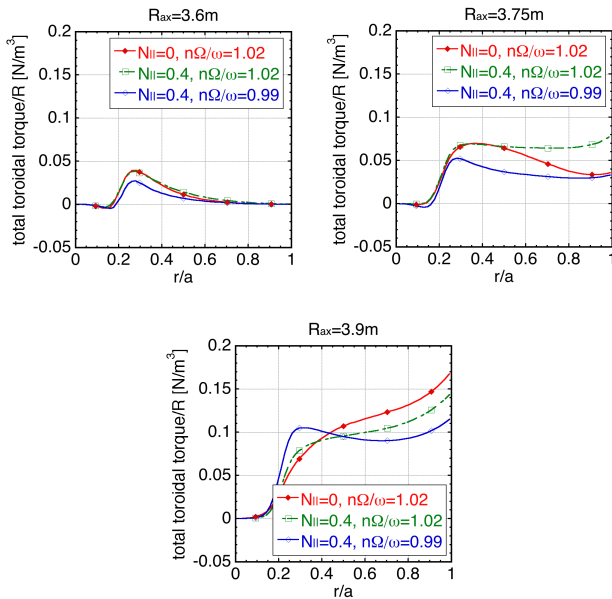


Fig. 5 The toroidal torque profiles with finite parallel refractive index ( $N_{\parallel} = 0.4$ ) in the three configurations.

of the worse confinement of supra-thermal electrons. For the outward shifted configuration, however, the integrated toroidal torque of heating at outer minor radii decrease because of the boundary.

When the ECH is injected obliquely, the parallel refractive index can have a finite value. The finite  $N_{\parallel}$  makes the shift of the resonance line in velocity space and modifies the heating source as shown in Fig. 2. We show the change of the toroidal torque due to different  $N_{\parallel}$  in Fig. 5. Assuming the ECH injection from the upper port in LHD

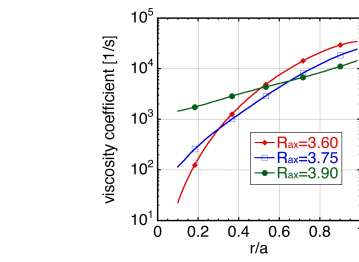


Fig. 6 The neoclassical viscosity coefficients in the three LHD configurations.

to the magnetic ripple bottom, the parallel refractive index is  $N_{\parallel} = 0.4 \sim 0.6$ . Also, the parameter  $n\Omega_{ce}/\omega$ , which is a parameter close to unity and must be greater than unity in the case of  $N_{\parallel} = 0$ , can be less than unity because of the Doppler effect. We compare the toroidal torque profiles by heating at the magnetic ripple bottom with parameters ( $n\Omega_{ce}/\omega = 1.02$ ,  $N_{\parallel} = 0$ ), ( $n\Omega_{ce}/\omega = 0.99$ ,  $N_{\parallel} = 0.4$ ) and ( $n\Omega_{ce}/\omega = 1.02$ ,  $N_{\parallel} = 0.4$ ). As a result, the obliquely injected ECH can change the toroidal torque up to about 40% as the integrated toroidal torque. To determine the parameter  $n\Omega_{ce}/\omega$ , we need to apply a ray-tracing simulation and precisely obtain the magnetic field strength of the ECH power absorption position, but this is beyond the scope of this paper.

We evaluate the toroidal flow  $V(r)$  driven by ECH torque, solving the diffusion equation

$$\frac{\partial V(r)}{\partial t} = \frac{1}{r} \frac{\partial}{\partial r} \left( rD \frac{\partial V(r)}{\partial r} \right) + \frac{T(r)}{m_i n_i R} - \mu(r)V(r), \quad (5)$$

where  $T$ ,  $D$  and  $\mu$ , are the ECH torque, the diffusion coefficient and the viscosity coefficient, respectively. The toroidal momentum is driven by the ECH torque and modified by the neoclassical toroidal viscosity. The radial flux of the toroidal momentum is balanced by the turbulence-driven flux, which consists of the convective flux and the Reynolds stress. The convective flux is usually considered to be ignorable and the Reynolds stress can be expressed as the diffusive and the non-diffusive terms. Here, we take only the diffusive term into account for simplicity. The diffusion coefficient is estimated experimentally, and it is of the order of unity [13]. The viscosity coefficient is evaluated as [14]

$$\mu \approx \pi^{1/2} \langle (\hat{\mathbf{n}} \cdot \nabla \mathbf{B})^2 / B^2 \rangle (R/M) (2eT_i/m_i). \quad (6)$$

The viscosity coefficients in the three configurations are shown in Fig. 6 The obtained toroidal torque is the largest in the outward shifted configuration, while the viscosity coefficient near the axis is the largest in the outward shifted configuration. The outward shifted configuration has the strong driving and damping forces. On the other hand, the inward shifted configuration has the weak driving and damping forces. Their effects conflict. We investigate the toroidal flows in the three configurations. The steady

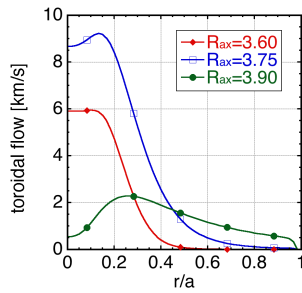


Fig. 7 The toroidal flow velocities obtained by solving the diffusion equation in the three LHD configurations.

toroidal flows driven by heating near the axis  $r/a \sim 0.1$  are shown in Fig. 7. As a result, toroidal flow in the standard configuration is the largest with the same input parameter ( $D = 1\text{m}^2/\text{s}$ ,  $P = 1\text{MW}$ ) because of its small viscosity and large toroidal torque. The second largest toroidal flow is obtained in the inward shifted configuration, which has the smallest viscosity coefficient around the axis in the three configurations.

#### 4. Conclusions

We have evaluated the ECH torque, which consists of the  $j_r \times B$  and collisional torques, in LHD plasmas by applying the GNET code to investigate the magnetic configuration and heating location dependences of the toroidal torque. In a non-symmetric configuration, the  $j_r \times B$  torque can be larger than the collisional torque and generate the net torque. The  $j_r \times B$  torque is caused by the radial electron current driven by ECH, which is subject to the radial drift velocity of trapped electrons accelerated by ECH and the fraction of trapped electrons.

Heating at the ripple bottom makes more trapped electrons and thus generates larger toroidal torque than heating at the ripple top. The supra-thermal electrons heated by ECH need pitch angle scattering before they get trapped in the ripple top heating case. Heating at the outer minor radius generates larger torque than heating at the inner minor radius due to the strong magnetic ripple. Also, obliquely injecting the EC wave can change the toroidal torque.

The inward shifted configuration has better confinement of supra-thermal electrons than that of the outward shifted configuration. This indicates that the radial velocity of supra-thermal electrons is faster in the outward shifted configuration and generate a larger radial electron current by ECH. Therefore, the outward shifted configuration makes the largest toroidal torque when the ECH heating location is near the axis. When the heating location is set at outer minor radii, the net torque decreases because of the boundary.

Finally, we have evaluated the toroidal flow with obtained toroidal torques, by solving the diffusion equation. The driving force, i.e., the ECH torque, is the largest in the

outward shifted configuration, although the damping force, i.e., the neoclassical viscosity, is the largest in the outward shifted configuration, too. As a result, the obtained toroidal flow is the largest in the standard configuration because of its small viscosity and large toroidal torque. Also, the second largest toroidal flow is in the inward shifted configuration, which has the smallest viscosity coefficient of the three configurations.

#### Acknowledgments

The authors thank LHD Experiment Group for their excellent support of this work. This work was supported by JSPS KAKENHI Grant Numbers JP18K03582. This work is also supported by the National Institute for Fusion Science grant administrative budget (NIFS10ULHH021) and the NIFS Collaboration Research program (NIFS19KNST150).

- [1] M. Yoshida, Y. Kamada, H. Takenaga, Y. Sakamoto, N. Oyama, H. Urano and the JT-60 Team, Nucl. Fusion **49**, 115028 (2009).
- [2] S.T.A. Kumar, J.N. Talmadge, T.J. Dobbins, F.S.B. Anderson, K.M. Likin and D.T. Anderson, Nucl. Fusion **57**, 036030 (2017).
- [3] P.H. Diamond, Y. Kosuga, Ö.D. Gürçan, C.J. McDevitt, T.S. Hahm, N. Fedorczak, J.E. Rice, W.X. Wang, S. Ku, J.M. Kwon, G. Dif-Pradalier, J. Abiteboul, L. Wang, W.H. Ko, Y.J. Shi, K. Ida, W. Solomon, H. Jhang, S.S. Kim, S. Yi, S.H. Ko, Y. Sarazin, R. Singh and C.S. Chang, Nucl. Fusion **53**, 104019 (2013).
- [4] M. Yoshinuma, K. Ida, M. Yokoyama, M. Osakabe and K. Nagaoka, Fusion Sci. Technol. **58**, 375 (2010).
- [5] K. Ida, S. Kado and Y. Liang, Rev. Sci. Instrum. **71**, 2360 (2000).
- [6] Y. Yamamoto, S. Murakami, C.C. Chang, H. Takahashi, K. Ida, M. Yoshinuma, W.H. Ko and the LHD Experiment Group, Nucl. Fusion (submitted).
- [7] Y. Yamamoto, S. Murakami, C.C. Chang, S.T.A. Kumar, J.N. Talmadge, K. Likin and D.T. Anderson, Plasma Fusion Res. **14**, 3403105 (2019).
- [8] S. Murakami, U. Gasparino, H. Idei, S. Kubo, H. Maassberg, N. Marushchenko, N. Nakajima, M. Romé and M. Okamoto, Nucl. Fusion **40**, 693 (2000).
- [9] M. Romé, V. Erckmann, U. Gasparino, H.J. Hartfuß, GKüher, H. Maaßberg and N. Marushchenko, Plasma Phys. Control. Fusion **39**, 117 (1997).
- [10] S. Hasegawa, S. Murakami and Y. Moriya, Plasma Fusion Res. **8**, 2403083 (2013).
- [11] M.N. Rosebluth and F.L. Hinton, Nucl. Fusion **36**, 55 (1996).
- [12] A. Snicker, O. Asunta, H. Ylitie, T. Kurki-Suonio, M. Schneider and S.D. Pinches, Nucl. Fusion **55**, 063023 (2015).
- [13] K. Ida, H. Lee, K. Nagaoka, M. Osakabe, C. Suzuki, M. Yoshinuma, R. Seki, M. Yokoyama, T. Akiyama and LHD Experiment Group, Phys. Rev. Lett. **111**, 055001 (2013).
- [14] K. Ida and N. Nakajima, Phys. Plasmas **4**, 310 (1997).